Proceedings of the XII International Symposium on Dynamic Problems of Mechanics (DINAME 2007),
P.S.Varoto and M.A.Trindade (editors), ABCM, Ilhabela, SP, Brazil, February 26 - March 2, 2007

Dynamic Characteristics of Aerostatic Ceramic Porous Bearings

Rodrigo Nicoletti, Zilda C. Silveira, and Benedito M. Purquerio

University of São Paulo, Engineering School of São Carlos, Department of Mechanical Engineering
Av. Trabalhador São-Carlense, 400, São Carlos - SP, 13566-590, Brazil
E-mail: rnicolet@sc.usp.br; silveira@sc.usp.br; purqerio@sc.usp.br.

Abstract: The advantage of adopting ceramic materials to build the bearing casings of ultra precision machines lies on the fact that these materials present high resistance to wear and temperature, which can be severe under the high velocity and low bearing gap conditions of such machines (bearing gap below 20 microns and spindle rotating velocity above 10,000 rpm). In this work, an aerostatic bearing with porous ceramic bearing case is proposed and analyzed. The governing equation of the bearing (modified Reynolds equation) is presented considering not only the axial and tangential air velocity profiles in the bearing gap (aerodynamic effects), but also the radial air velocity profile of the injected air through the capillary porous all over the bearing sliding surface (aerostatic effects). By integrating the modified Reynolds equation, the static and dynamic characteristics of the system are analyzed as function of adimensional parameters. The results show that the adimensional parameter related to porous medium (Γ) strongly affects the load capacity and stiffness of the bearing. A case study in a grinding machine spindle is also performed, where static and dynamic deflection maps are presented as a function of the bearing supply pressure, grinding force and depth of cut, helping defining the best operational ranges of the grinding machine.

Keywords: aerostatic bearings, porous ceramic, modified Reynolds equation, ultra precision machines.

NOMENCLATURE

a = distance from bearing to tool, m
b = distance between bearings, m
c = assembled clearance, m
d = damping coefficient, $N.s/m$
$\mathbf{D}$ = damping matrix
$\bar{d} = (2\omega c)/(L_a L_t P_s)$ = adimensional damping
F = aerostatic/aerodynamic force, N
$\bar{F} = 2F/(L_a L_t P_s)$ = adimensional force
$\mathbf{G}$ = gyroscopic matrix
h = bearing clearance, m
$\bar{h} = h/c$ = adimensional clearance
$H = r_o - r_i$ = porous matrix thickness, m
k = stiffness coefficient, N/m
$\bar{k} = (2c)/(L_a L_t P_s)$ = adimensional stiffness
$\mathbf{K}$ = stiffness matrix
k_1 = permeability viscous coeffic., m^2
L_a = bearing width, m
$L_t = 2\pi r_i$ = bearing tangential length, m
$\mathbf{M}$ = inertia matrix
p = air film pressure, N/m^2
$\bar{p} = p/P_s$ = adimensional pressure
P_s = air supply pressure, N/m^2
R = rotor radius, m
r = porous bearing radius, m
t = time, s
u, v, w = fluid velocity profiles, m/s
U = rotor surface velocity, m/s
V_{inj} = air injection velocity, m/s
X, Y, Z = global coordinate system, m

Greek Symbols

$\Gamma = (12 k_1 L_t^2)/(c^3 H)$ = porous matrix adimensional parameter
δ = deflection at tooling edge, m
ε = rotor eccentricity, m
$\bar{\varepsilon} = \varepsilon/c$ = adimensional eccentricity
ζ = axial direction coordinate, m
$\bar{\zeta} = 2\zeta/L_a$ = adimensional coordinate
η = tangential direction coordinate, m
$\bar{\eta} = \eta/L_t$ = adimensional coordinate
$\Lambda = (12\mu\omega L_t^2)/(c^2 P_s)$ = excitation adimensional parameter
μ = air dynamic viscosity, $N.s/m^2$
ξ = radial direction coordinate, m
$\tau = \omega t$ = adimensional time
$\Psi = (6\mu U L_t)/(c^2 P_s)$ = rotating velocity adimensional parameter ω = excitation frequency, rad/s
Ω = shaft rotating velocity, rad/s

INTRODUCTION

Machines and processes related to ultra precision are those capable to manufacture a component with a precision of 1 μm and a resolution of 1 nm. The need for such tolerance ranges has been stimulated by the great demand of microelectronic and micro-electromechanical components. The performance of a ultra precision machine tool depends on the static and dynamic behavior of the mechanical subsystems that compose it. Among them, the bearing-shaft pair is essential to the quality of the manufacturing process. Such important parameters as the control of the precision of rotation, the repeatability of movements, and the machine load capacity depend on the bearing-shaft pair characteristics.

The bearing is an important component in the definition of the dynamic characteristics of rotating machines because it is the interface element between the rotor and the other components of the machine (static parts and ground). Hence, the operational range of the machine, which depends on the machine dynamic characteristics, will be defined by the appropriated design of the bearings (Hamrock, 2004; Nicoletti and Santos, 2005). The design and construction of the bearing-shaft pair are strongly related to dimensional conformity and quality of the component sliding surfaces, due to elastic bending of the shaft and deflection of the bearings (Balestrero, 1997). According to Cheng and Rowe (1995), the selection of the type of bearing basically depends on the type of application and the necessary operational parameters (stiffness, high speed, low friction, repeatability of movements and resistance to high temperatures). The air bearings, when compared

with others kinds of bearings such as the oil-lubricated bearings and the rolling bearings, have the advantage of offering low heat generation, practically no contamination, and high precision of movements (Lo et al, 2005). Externally pressurized air bearings held the characteristics of low noise, friction reduction and low heat generation, which is an indication for applications that require high precision in high speeds (Powell, 1970).

Due to the low viscosity of the air, externally pressurized air bearings tend to be unstable. The choice of restriction type in the air feeding can reduce this problem, and define the operation range and load capacity of the bearing. An alternative way to improve the stability of the air film and to increase the bearing stiffness is the use of non-metallic materials in the casing, e.g. porous ceramic materials. This design solution presents some additional advantages, such as low manufacturing cost, low material density, low wear due to abrasion, high dimensional stability, high chemical inertia, and tend to result in bearings with equal, or even higher, stiffness than those built with pockets or inherent orifices (Balestrero, 1997). Another important property of the ceramic materials is the machinability, where no ductile deformation and porous re-covering occurs, because of the porous characteristics (open porous).

In this paper, an aerostatic ceramic porous bearing is studied. The modified Reynolds equation is presented by considering the Darcy's equation of porous media applied to air journal bearings. The formulation is numerically solved by finite differences to determine the pressure distribution profile of the air film, the bearing load capacity, and bearing equivalent stiffness and damping coefficients, as a function of the adimensional parameters of the modified Reynolds equation. In extension, the proposed ceramic porous bearing is applied to the spindle of a grinding machine, where static analysis (deflection and flexibility of shaft edge) and dynamic analysis (frequency response functions) are performed, in order to define the best operational ranges of the machine.

Literature Review

Literature provides many works related to the dynamic identification of externally pressurized bearings. For instance, Sinhasan et al. (1989) investigated the effects of bearing shell deformation on the static and dynamic performance characteristics of a four-pocket capillary-compensated hydrostatic journal bearing. This study stated that, to establish an optimum design for the capillary-compensated hydrostatic journal bearing system, in order to support a particular external load, a carefully selection of the geometry of bearing and capillary restrictor is necessary, as a function of the modulus of elasticity of bearing material, supply pressure, thickness of bearing shell and radial clearance. Roblee and Mote Jr. (1990) proposed a design method for flat and circular thrust gas bearings based on a dynamic model. This study presented a selection strategy of stiffness and damping for high vibration environment applications. The poorly damped results of the external pressurized gas bearing are attributed to the fact that these bearings exhibit damping only over a narrow frequency range. In many applications, the damping of the machine is more important than the static stiffness of its bearings. According to the authors, there is a compromise between high static stiffness and the values of damping in the gas bearing performance.

Sun (1975) presented a linear model of gas-lubricated porous journal bearings, which combines the analytical solution of whirl instability to the journal rotation and pneumatic hammer effects associated to the external pressurization. His results are presented in terms of the variation of stability parameters, such as the threshold mass, the whirl frequency ratio associated to compressibility number and eccentricity ratio. In the results, it was observed that when the permeability parameter is zero, the analysis reduces to the case of a plain journal bearing. If the permeability increases from zero, the nature of instability changes from a condition of hydrodynamic whirl to one that is basically hybrid. The pneumatic hammer effect is identified as being inversely proportional to bearing compressibility number (Λ).

Majumdar (1976) proposed a design procedure to externally pressurized gas-lubricated metallic porous journal bearing considering static loading. The static behavior is related to the effect of the feeding parameter. These studies verified that the load capacity reaches a maximum value and decreases with further increase in feeding parameter (Γ). Yoshimoto and Kohno (2001) studied aerostatic circular porous thrust bearings built with graphite porous material. Two feeding systems were used: the annular grove air supply method and the orifice air supply method. In this study, it was observed that the shape of supply area has little influence on the static stiffness when the outer diameter of the supply area remains the same. The load capacity and damping coefficient of aerostatic thrust bearing with a restricted layer depends on the dimensionless parameter that is related to the permeability coefficient in radial direction and thickness of porous material. Fourka and Bonis (1995) investigated externally pressurized gas thrust bearings with different orifice and porous feeding systems. The authors compared the optimum characteristics regarding load capacity, stiffness and flow rate of an air thrust bearing using different kinds of multiple inlets designed with orifices or porous compensation. The study indicated that a better performance may be achieved for each feeding system, which depends on an optimum number of inlets, positioning of orifices or permeability coefficient of the porous material. Balestrero (1997) compared the bearing load capacity and stiffness of two aerostatic bearings using pocket orifice restrictors and porous inserts. The results indicated a best performance for the bearing with porous inserts regarding both load capacity and stiffness. The achieved bearing stiffness was 120 $N/\mu m$ for the bearing with pocket orifice restrictors and 300 $N/\mu m$ for the bearing with porous inserts.

Plante et al. (2005) presented a design model for a circular porous air bearing using one-dimensional generalized flow theory focusing on the essential physical phenomena governing the airflow. The authors compared the results of the

one-dimensional model to the results generated by the three-dimensional model, regarding force versus bearing gap and corresponding flow rates. The conclusion was that the one-dimensional model had a good agreement with experimental data, because the physics of the flow in the porous media was properly considered. Majumdar (1973) presented a theoretical procedure to derive the steady-state performance characteristics of stationary and rotating journals, by considering a three-dimensional flow in the porous material of a bearing. In this way, he demonstrated that the dynamic characteristics of the gas film is fundamental to response of gas bearing supported systems and that the important parameters are the film stiffness, the damping, and the stability range. Majumdar (1980), on the other hand, presented a literature review on theoretical models to obtain stiffness and damping values of external pressurized, rectangular and porous thrust bearings.

The geometry and intercommunication of the pores in advanced ceramics has direct correspondence to the permeability property of the material, which is represented by the permeability viscous coefficient (k_1) considering laminar flow in the fluid. Kwan and Corbett (1998a,1998b), Fourka and Bonis (1995) and Yoshimoto and Kohno (2001) cite values of permeability viscous coefficients between 10^{-16} and 10^{-12} m^2 in experimental and numerical studies. The work of Kwan and Corbett (1998a) involves the determination of permeability inertial coefficients and the effect of the slip velocities in the porous media of air bearings, considering turbulent flow as well as surface roughness. This value estimation is essential to design porous ceramic bearings that present acceptable operation range of high stiffness and damping.

MATHEMATICAL MODELLING

The aerostatic ceramic porous bearing in study is a plain journal bearing whose casing is made of porous ceramic material (Fig. 1). Pressurized air at pressure P_s is injected into the bearing gap (h) trough the porous of the ceramic matrix (H) that composes the bearing casing, thus forming an aerostatic pressure distribution in the bearing gap.

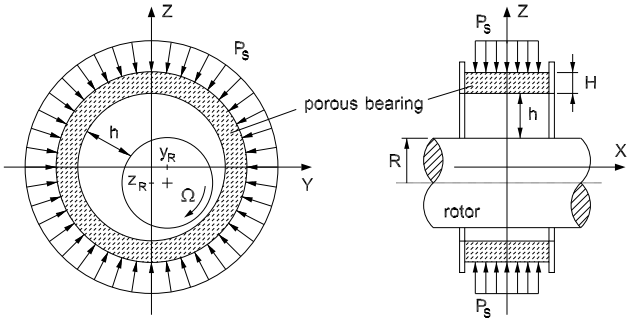

Figure 1 – Schematic view of the aerostatic ceramic porous bearing.

In order to calculate the aerostatic pressure distribution in the bearing gap, one assumes that the fluid is isoviscous, Newtonian, incompressible, and operating in the laminar regime. Thus, one can simplify the Navier-Stokes equations, and rewrite them in the reference frame fixed in the bearing, supposing that the considered bearing area for analysis is part of a shallow and long channel (Fig. 2). The fluid flow nonslip boundary conditions in the bearing gap, shown in Fig. 2, are given by:

$$\begin{aligned} &u(\zeta,\eta,0) = V_{inj} \qquad v(\zeta,\eta,0) = 0 \qquad w(\zeta,\eta,0) = 0 \\ &u(\zeta,\eta,h) = \frac{\partial h}{\partial t} \qquad v(\zeta,\eta,h) = U = R\Omega \qquad w(\zeta,\eta,h) = 0 \end{aligned} \tag{1}$$

Integrating the Navier-Stokes equations subjected to the nonslip boundary conditions (Eq.(1)), one gets the expressions for the fluid velocity profiles in the bearing gap shown in Fig. 2:

$$\begin{cases} u(\xi) = \dfrac{\xi}{h}\dfrac{\partial h}{\partial t} + \left(\dfrac{h-\xi}{h}\right) V_{inj} \\ v(\xi) = \dfrac{1}{2\mu}\dfrac{\partial p}{\partial \zeta}\left(\xi^2 - h\xi\right) + \dfrac{U}{h}\xi \\ w(\xi) = \dfrac{1}{2\mu}\dfrac{\partial p}{\partial \zeta}\left(\xi^2 - h\xi\right) \end{cases} \tag{2}$$

Inserting the expressions for the fluid velocity profiles (Eq.(2)) into the continuity equation, and integrating it between the limits $[0,h]$, one obtains the modified Reynolds equation as a function of the injection velocity V_{inj}, as follows:

$$\frac{\partial}{\partial \eta}\left(\frac{h^3}{\mu}\frac{\partial p}{\partial \eta}\right) + \frac{\partial}{\partial \zeta}\left(\frac{h^3}{\mu}\frac{\partial p}{\partial \zeta}\right) = 6U\frac{\partial h}{\partial \eta} + 12\frac{\partial h}{\partial t} - 12V_{inj} \tag{3}$$

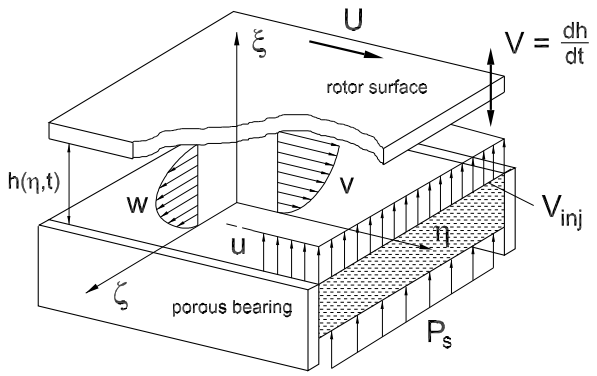

Figure 2 – Fluid flow kinematics, velocity profiles and nonslip boundary conditions in the bearing gap.

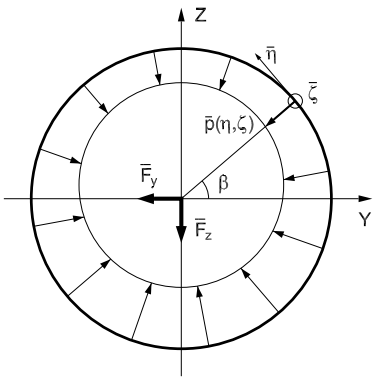

Figure 3 – Aerostatic/aerodynamic forces acting on the shaft.

The injection velocity can be estimated by the linearized Darcy equation, which relates the injection velocity with the pressure difference between opposite sides of the porous medium:

$$\frac{\mu}{k_1} V_{inj} = \frac{\Delta p}{H} = \frac{P_s - p}{r_o - r_i} \tag{4}$$

Hence, by inserting Eq.(4) into Eq.(3), and manipulating it, one obtains the modified Reynolds equation as a function of the porous bearing parameters, as follows:

$$\frac{\partial}{\partial \eta}\left(\frac{h^3}{\mu}\frac{\partial p}{\partial \eta}\right) + \frac{\partial}{\partial \zeta}\left(\frac{h^3}{\mu}\frac{\partial p}{\partial \zeta}\right) - \frac{12 k_1}{\mu (r_o - r_i)} p = 6U\frac{\partial h}{\partial \eta} + 12\frac{\partial h}{\partial t} - \frac{12 k_1 P_s}{\mu (r_o - r_i)} \tag{5}$$

Equation (5) can be written in adimensional form, resulting in the following expression:

$$\frac{\partial}{\partial \bar{\eta}}\left(\bar{h}^3\frac{\partial \bar{p}}{\partial \bar{\eta}}\right) + \left(\frac{2L_t}{La}\right)^2 \frac{\partial}{\partial \zeta}\left(\bar{h}^3\frac{\partial \bar{p}}{\partial \zeta}\right) - \Gamma \bar{p} = \Lambda\frac{\partial \bar{h}}{\partial \bar{\eta}} + \Psi\frac{\partial \bar{h}}{\partial \tau} - \Gamma \tag{6}$$

where:

$$\Gamma = \frac{12 k_1 L_t^2}{c^3 H} \qquad \Lambda = \frac{6\mu U L_t}{c^2 P_s} \qquad \Psi = \frac{12\mu\omega L_t^2}{c^2 P_s} \tag{7}$$

The pressure distribution in the bearing gap can be calculated by integrating the modified Reynolds equation (Eq.(5) or Eq.(6)). Both aerodynamic and aerostatic effects are computed by these equations, although the aerodynamic effects be very small compared to the aerostatic ones due to low viscosity of the fluid. In Eq.(6), the adimensional parameter Λ is related to the shaft rotating velocity; the adimensional parameter Ψ is related to the radial excitation frequency of the shaft; and the adimensional parameter Γ is related to the porous medium characteristics of the bearing casing. By setting these parameters, one can achieve specific pressure distributions in the bearing gap, thus affecting the resultant dynamic characteristics of the bearing.

The aerostatic/aerodynamic forces acting on the shaft can be calculated by integrating the pressure distribution in the inner surface area of the bearing casing (Fig.3):

$$\begin{aligned} \bar{F_y} &= -\int_{-1}^{1}\int_{0}^{1} \bar{p}\cos\beta \; d\bar{\eta}\, d\bar{\zeta} \\ \bar{F_z} &= -\int_{-1}^{1}\int_{0}^{1} \bar{p}\sin\beta \; d\bar{\eta}\, d\bar{\zeta} \end{aligned} \tag{8}$$

By calculating the aerostatic/aerodynamic forces acting on the shaft, one can estimate the dynamic coefficients of the bearing (stiffness and damping), and analyze the bearing dynamic characteristics.

NUMERICAL RESULTS

The adimensional modified Reynolds equation (Eq.(6)) is integrated by adopting the Finite Difference Method. Ambient pressure is considered at the bearing edges (null boundary condition). By solving the adimensional modified Reynolds

equation, one obtains the pressure distribution in the bearing gap. By integrating the pressure distribution (Eq.(8)), one calculates the bearing forces acting on the rotor (shaft). The static equilibrium position of the rotor in the bearing results from the balance of forces between the aerostatic/aerodynamic forces and the external forces acting on the shaft. The equivalent dynamic coefficients of the bearing are calculated by a simplification of the perturbation method proposed by Allaire et al. (1981), considering a fixed pad configuration of the bearing.

Influence of Adimensional Parameters Γ, Λ and Ψ

In this section, one investigates the influence of the adimensional parameters of the modified Reynolds equation (Eq.(6)) on the bearing load capacity and equivalent dynamic coefficients. The adopted operational conditions are listed in Tab. 1.

Table 1 – Geometric characteristics and operational conditions of the porous bearing.

Constant Parameters	Variation of Γ	Variation of Λ	Variation of Ψ
$c = 15\ \mu m$	$1\times10^{-14} < k_1 < 5\times10^{-10}\ m^2$	$k_1 = 3\times10^{-14}\ m^2$	$k_1 = 3\times10^{-14}\ m^2$
$H = 20\ mm$	$\Omega = 250\ Hz$	$20 < \Omega < 500\ Hz$	$\Omega = 250\ Hz$
$R = 25\ mm$	$\omega = 10\ Hz$	$\omega = 10\ Hz$	$5 < \omega < 100\ Hz$
$\mu = 1.8\times10^{-5}\ N.s/m^2$	$43.9 < \Gamma < 2.2\times10^{6}$	$\Gamma = 131.75$	$\Gamma = 131.75$
$P_s = 2.0\ MPa$	$\Lambda = 1.48$	$0.118 < \Lambda < 2.96$	$\Lambda = 1.48$
	$\Psi = 0.745$	$\Psi = 0.745$	$0.372 < \Psi < 7.45$

Figure 4 presents the results of bearing load capacity as a function of the adimensional parameters Γ, Λ and Ψ. In this case, the bearing load capacity is the necessary force to zero the gap between the rotor and the bearing surface ($\bar{\varepsilon} = 1$). As one can see in Fig. 4(a), the parameter Γ have a strong influence on the bearing load capacity. The maximum value of load capacity is achieved for $\Gamma = 65.9$, but as Γ increases, the bearing load capacity presents a strong reduction. There is also a reduction in load capacity for $\Gamma < 65.9$. Considering that Γ is the parameter that contains information of the bearing porosity, the choice of k_1 and H play an important role in defining the parameter Γ, and consequently the bearing load capacity, as one can see in Fig. 4(a).

The effect of parameter Λ in the bearing load capacity is much lower than that of parameter Γ (Fig. 4(b)). As Λ increases, there is a small increase of bearing load capacity. This is caused by the fact that Λ is the parameter related to the shaft rotating velocity ($U = R\Omega$). As the rotating velocity of the shaft increases, the aerodynamic effects in the air film also increase (air film pressure increases), thus positively affecting the load capacity. Considering that the aerostatic effects are predominant in the bearing in study, it is not a surprise that the aerodynamic effects cause such a slight change in the load capacity.

As one can see in Fig. 4(c), the parameter Ψ has no effect on the bearing load capacity (constant load capacity). The parameter Ψ is related to the excitation frequency that the shaft is subjected (ω), which is a dynamic quantity. Considering that the bearing load capacity is a static quantity, it is clear that the bearing load capacity does not depend on the shaft excitation frequency.

Figure 5 presents the results of bearing stiffness as a function of the adimensional parameters Γ, Λ and Ψ. As one can see in Fig. 5(a), the bearing stiffness is strongly affected by the parameter Γ. A maximum value of the bearing stiffness is achieved for $\Gamma = 131.8$. Similarly to the load capacity case, the choice of k_1 and H play an important role in defining the parameter Γ, and consequently the bearing equivalent stiffness.

As one can see in Fig. 5(b), the direct stiffness coefficients ($\bar{k}_{yy}$ and $\bar{k}_{zz}$) are not influenced by the parameter Λ, which is related to the rotating velocity of the shaft. The increase of air film aerodynamic effects does not contribute to the direct stiffness of the bearing, but only to the cross coupling coefficients ($\bar{k}_{yz}$ and $\bar{k}_{zy}$). Considering that the bearing stability is strongly related to the values of cross coupling coefficients, care must be taken during bearing design in the choice of parameter Λ.

The parameter Ψ does not affect the bearing stiffness, as one can see in Fig. 5(c). Again, parameter Ψ is related to the excitation frequency that the shaft is subjected, which is a dynamic quantity. Considering that the bearing stiffness is a static quantity, it is clear that the bearing load capacity does not depend on the shaft excitation frequency.

Figure 6 presents the results of bearing damping as a function of the adimensional parameters Γ, Λ and Ψ. The obtained cross coupling damping coefficients ($\bar{d}_{yz}$ and $\bar{d}_{zy}$) are very close to zero and can be neglected. As one can see in Fig. 6(a), the bearing direct damping ($\bar{d}_{yy}$ and $\bar{d}_{zz}$) is strongly affected by the parameter Γ. As Γ increases, the bearing damping presents a strong reduction. Similarly to the load capacity and stiffness cases, the choice of k_1 and H play an important role in defining the bearing equivalent damping.

Parameter Λ does not affect the bearing damping coefficients, as one can see in Fig. 6(b). Parameter Λ is related to the rotating velocity of the shaft, which increases the air film aerodynamic effects. It is clear, however, that the bearing damping does not depend on the shaft rotating velocity.

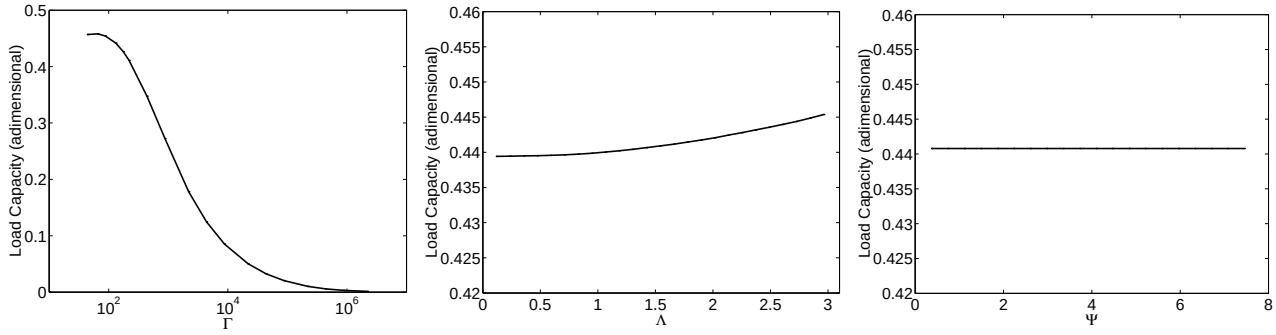

Figure 4 – Bearing load capacity as a function of the adimensional parameters Γ, Λ and Ψ.

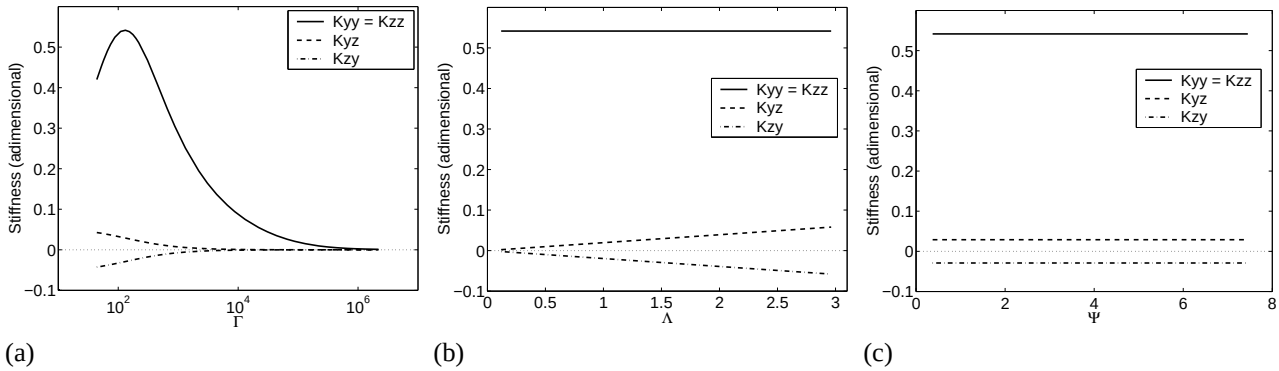

Figure 5 – Bearing equivalent stiffness as a function of the adimensional parameters Γ, Λ and Ψ ($\bar{\varepsilon} = 0$).

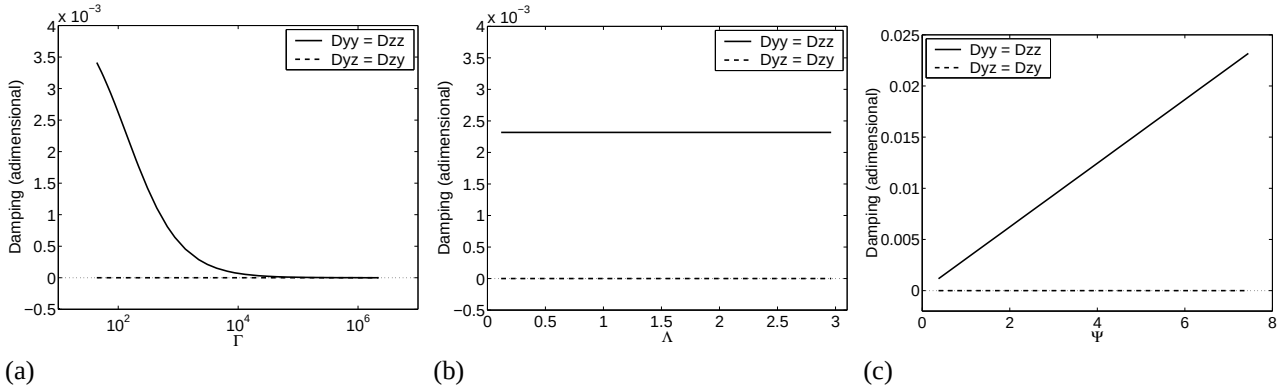

Figure 6 – Bearing equivalent damping as a function of the adimensional parameters Γ, Λ and Ψ ($\bar{\varepsilon} = 0$).

In Fig. 6(c), one can see that parameter Ψ has a strong influence on the direct damping coefficients ($\bar{d}_{yy}$ and $\bar{d}_{zz}$). These coefficients linearly vary as Ψ increases, and one achieves damping values much higher than those achieved with parameter Γ. Hence, the bearing damping can be set by properly choosing parameter Ψ.

It is important to note that Figs. 4 to 6 present results for null rotor eccentricity (rotor centered in the bearing), and different rotor eccentricities may alter the results. However, no significant changes in the bearing load capacity and dynamic coefficients are observed for eccentricities up to $\bar{\varepsilon} = 0.25$, which is the range for normal operation of such bearings.

Application to Grinding Machine Spindle

In order to investigate the dynamic behavior of a shaft supported by the ceramic porous bearing in study, one modeled the spindle of a Whitnon grinding machine (Fig. 7(a)). Originally, the spindle is supported by two aerostatic bearings, each one with two rows of twelve inherent orifices. In this study, the spindle is modeled by finite elements, adopting the flexible shaft elements proposed by Nelson and McVaugh (1976), and the bearings are modeled by the equivalent dynamic coefficients, calculated with the present theory (Fig. 7(b)). The ceramic porous bearing geometry was chosen in such a way that one achieves maximum stiffness, i.e. $100 < \Gamma < 150$, as shown in Fig 5(a). The chosen bearing parameters for

this analysis are: $R = 38\ mm$ (original shaft radius), $L_a = 96\ mm$ (original width of the bearings), $c = 25\ \mu m$, $H = 30\ mm$, and $k_1 = 10^{-13}\ m^2$, resulting in an adimensional parameter $\Gamma = 146.1$.

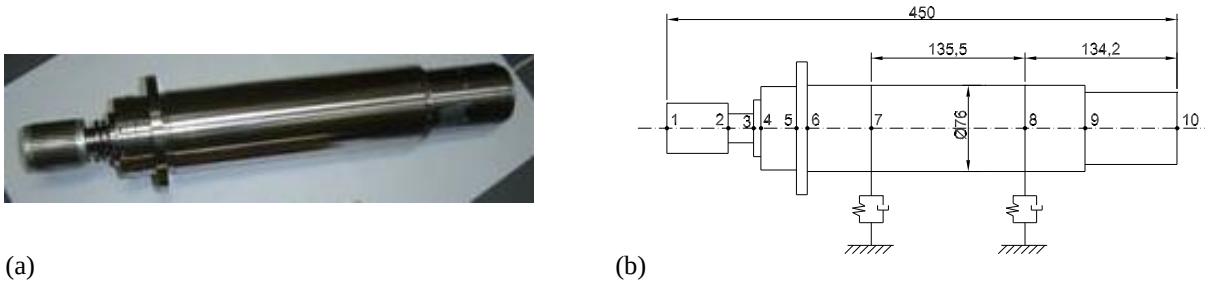

(a) (b)

Figure 7 – Grinding machine rotor spindle and equivalent model by flexible shaft elements.

As a reference for the involved forces in grinding procedures, one adopts the experimental data presented by Zhou et al. (1992). In their work, Zhou et al. (1992) studied the effects of radial grinding force and depth of cut in the resultant surface roughness of the work piece, by using a fine grit diamond wheel. Their results, shown in Fig. 8, are due to a wheel surface velocity of 1000 m/min (spindle velocity of 909 rpm), work piece surface velocity of 30 m/min, infeed rate of 6 $\mu m/min$, and depths of cut of 0.1, 0.4 and 1.2 μm.

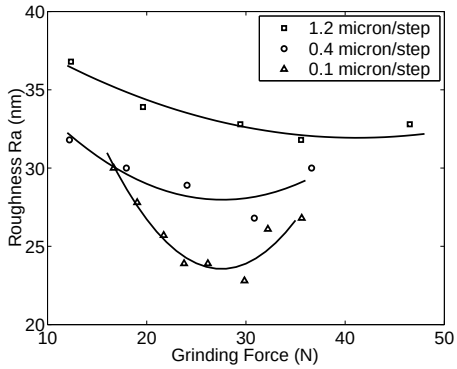

Figure 8 – Work piece surface roughness as a function of the grinding force and depth of cut (Zhou et al., 1992).

The spindle-bearing system must have proper static and dynamic characteristics to keep the maximum deflection at the grinding wheel of the spindle within the range of depth of cut, when subjected to the grinding forces. Once the maximum deflection at the grinding wheel, for a certain grinding force, remains within the range of depth of cut, one can achieve the expected surface finishing quality of the work piece, as shown in Fig. 8.

Static Analysis

The static deflection of the spindle at the grinding wheel location (node 10 - Fig. 7(b)) can be decomposed into the structural deflection and the rigid body deflection due to the bearings (Fig. 9). The structural deflection (δ_2) is caused by the inherent flexibility of the spindle material. To calculate this deflection, one uses the finite element model of the shaft, with rigid bearings (high stiffness at bearing locations) and a unitary force applied to the grinding wheel location. In this case, the obtained structural deflection rate of the spindle is $\delta_2/F = 5.47\ nm/N$.

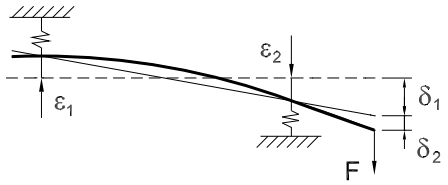

Figure 9 – Combined structural and bearing deflections.

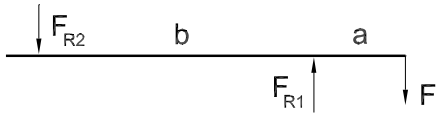

Figure 10 – Reacting forces in the bearings.

The rigid body deflection (δ_1) depends on the eccentricities at the bearings (ε_1 and ε_2), and on the distances a (bearing to grinding wheel) and b (between bearings), as follows:

$$\delta_1 = \left(\frac{a}{b} + 1\right)\varepsilon_1 + \frac{a}{b}\varepsilon_2 \tag{9}$$

The eccentricities at the bearings are obtained by calculating the equilibrium position of the shaft in the bearings, when subjected to the reaction forces (F_{R1} and F_{R2} - Fig. 10). The reaction forces are given by the following relationship:

$$F_{R1} = \left(\frac{a}{b} + 1\right) F \qquad F_{R2} = \frac{a}{b} F \tag{10}$$

Figure 11 presents the total static deflection ($\delta_1 + \delta_2$) of the spindle at grinding wheel location as a function of the bearing supply pressure (P_s) and grinding force. As one can see, the total static deflection is linearly proportional to the grinding force, but inversely proportional to the supply pressure. As the bearing supply pressure increases, the bearing stiffness also increases, resulting to lower eccentricities at the bearings and, consequently, lower rigid body deflections. As a result, the deflection ratio δ_2/δ_1 tends to increase as the supply pressure value increases (for $P_s = 0.3\,MPa$, $\delta_2/\delta_1 =$ 7.7%; for $P_s = 0.6\,MPa$, $\delta_2/\delta_1 = 14.7\%$; for $P_s = 1.0\,MPa$, $\delta_2/\delta_1 = 24.6\%$).

Considering the results presented by Zhou et al. (1992) (Fig. 8), one has three different depths of cut: 0.1, 0.4 and 1.2 μm. In order to achieve the expected surface roughness in the work piece, it is necessary to keep the total static deflection at the grinding wheel below these values. For that, a proper set of grinding force and bearing supply pressure values must be chosen. To help this task, one has the static deflection map shown in Fig 12.

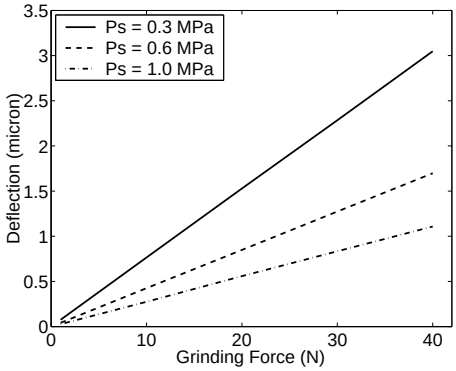

Figure 11 – Static deflection as a function of the force at the grinding wheel of the spindle.

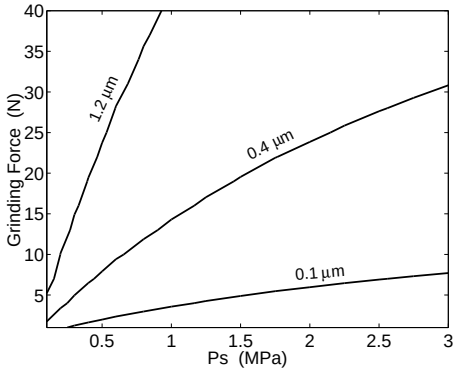

Figure 12 – Static deflection map as a function of the bearing supply pressure and force at the grinding wheel of the spindle.

As one can see in Fig. 12, given a certain value for the bearing supply pressure, there is a maximum acceptable value for the grinding force to keep the total static deflection below the desired value of depth of cut. In this case, it is possible to use a supply pressure of 1 *MPa* for the case of 1.2 μm depth of cut in the whole range of grinding forces (up to 40 *N*). On the other hand, a precision of 0.1 μm can only be achieved by adopting low grinding forces (below 10 *N*), and not for all possible values of supply pressure (only above 0.25 *MPa*).

Dynamic Analysis

Similarly to the static case, it is interesting to keep the dynamic deflections at the grinding wheel of the spindle below the value of depth of cut, in order to achieve the desired finishing quality at work piece surface. For that, one has to analyze the frequency response functions at the grinding wheel. By adopting the finite element model described above, one calculates the frequency response functions of the system as follows:

$$FRF = \frac{\delta_1 + \delta_2}{F} = \frac{1}{-\omega^2 \mathbf{M} - i\omega(\mathbf{D} - \Omega\mathbf{G}) + \mathbf{K}} \tag{11}$$

Figure 13 presents the frequency response and phase of the grinding wheel location of the spindle (node 10 of the model) as a function of the excitation frequency (ω) and bearing pressure supply (P_s). The bearing pressure supply causes the reduction of dynamic deflections by increasing the bearing stiffness. This can be clearly seen by comparing the results for low frequency ranges (up to 200 *Hz*), where one has lower responses (deflections) for higher supply pressures. In addition, the resonance peaks move to higher frequency values and also present a reduction in amplitude.

In order to keep the dynamic deflection below the value of depth of cut, one has to analyze the amplitude of grinding forces involved. For that, a proper set of grinding force and bearing supply pressure values must be chosen. To help this task, one has the dynamic deflection map shown in Fig 14. This map can be read by initially choosing the supply pressure (P_s) and the grinding force. Each map refers to a specific value of depth of cut (maximum allowable dynamic deflection). If the pressure supply is P_3 and the grinding force is F_2, then the system can be used for excitation frequencies between 0 and ω_5, and frequencies above ω_6 (Fig. 14(a)). If the pressure supply is P_2 and the grinding force is F_2, then the system can only be used for excitation frequencies above ω_4. However, this same supply pressure (P_2) can be used with the grinding

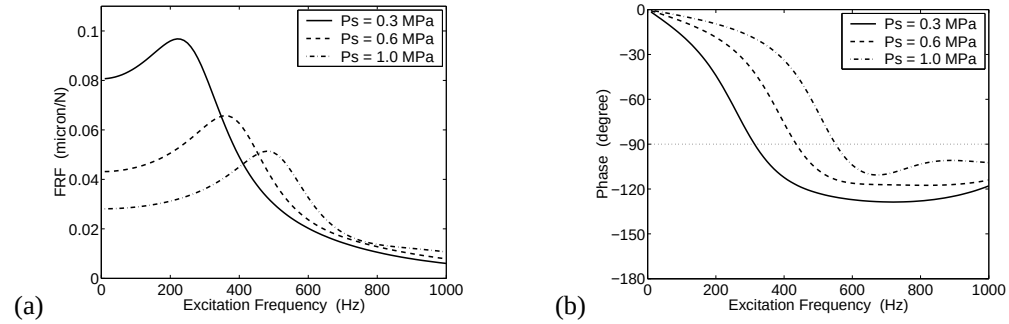

Figure 13 – Frequency response of the tooling edge of the spindle as a function of the excitation frequency and bearing supply pressure: (a) FRF; (b) Phase.

force F_1 in the whole range of frequencies. If the pressure supply is P_1 and the grinding force is F_1, then the system can be used for excitation frequencies between 0 and ω_1, and frequencies above ω_2. The supply pressure P_1 can only be used with grinding force F_2 for frequencies above ω_3.

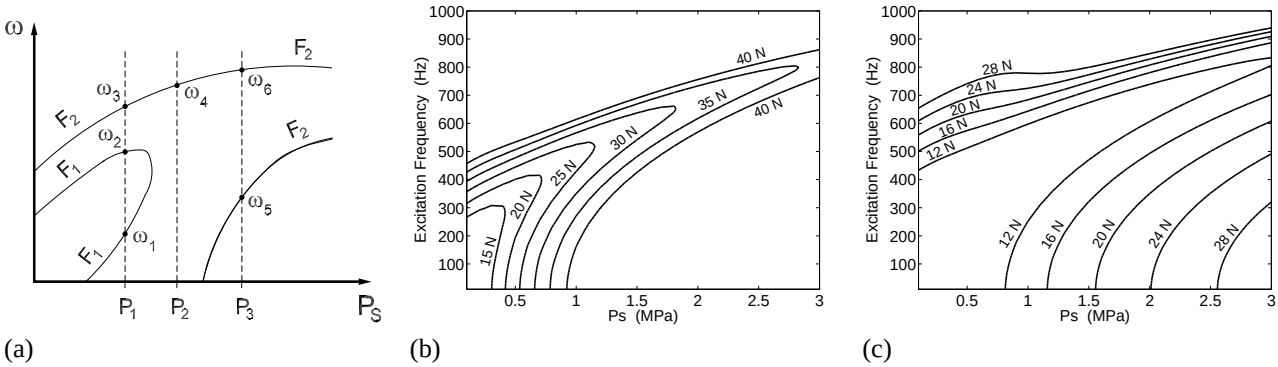

Figure 14 – Dynamic deflection map as a function of the bearing supply pressure and excitation frequency: (a) map view; (b) 1.2 μm depth of cut; (c) 0.4 μm depth of cut.

In Fig. 8, one can see that the minimum roughness values are obtained for grinding forces of 28 N (0.4 and 0.1 μm depths of cut) and 40 N (1.2 μm depth of cut). Figures 14(b) and 14(c) present the dynamic deflection maps for the values of depth of cut of 0.4 and 1.2 μm, respectively. Looking at Fig. 14(b) (1.2 μm depth of cut), one can see that it is possible to work at the optimum grinding force (40 N) using bearing supply pressures above 1 MPa. However, there is a limitation in the excitation frequency range, which depends on the adopted pressure (e.g. for $Ps = 1.0\ MPa$, $\omega < 160\ Hz$; for $Ps = 1.5\ MPa$, $\omega < 426\ Hz$; for $Ps = 2.0\ MPa$, $\omega < 568\ Hz$; and for $Ps = 3.0\ MPa$, $\omega < 763\ Hz$). A grinding force of 30 N results in surface roughness close to the minimum one (Fig. 8 for 1.2 μm). Analyzing Fig. 14(b) for 30 N, one can see that it is possible to work in the whole frequency range (from 0 to 1000 Hz) with supply pressures above 2 MPa.

In Fig. 14(c) (0.4 μm depth of cut), one can see that it is not possible to work in the whole frequency range (0 to 1000 Hz). There is always a limitation in frequency, whatever the grinding force or supply pressure be. This is caused by the smaller value of the depth of cut, which strongly restricts the maximum dynamic deflection of the spindle. For the optimum grinding force (28 N), only large supply pressures can be used (above 2.5 MPa), with small frequency ranges ($\omega < 300\ Hz$). A grinding force of 20 N results in surface roughness close to the minimum one (Fig. 8 for 0.4 μm). Analyzing Fig. 14(c) for 20 N, one can see that it is possible to work in larger frequency ranges (up to 500 Hz) with supply pressures above 1.5 MPa.

No dynamic deflection map is presented for the 0.1 μm depth of cut because this value is too small for the system is study. Under the adopted operational conditions, the system cannot present dynamic deflections below 0.1 μm, thus representing a limitation in the use of such technology in these machines.

CONCLUSIONS

In this work, the modified Reynolds equation for a ceramic porous bearing is presented, and the static and dynamic characteristics of the system are analyzed as function of adimensional parameters. One can conclude that the adimensional parameter related to the porous medium (Γ) strongly affects the load capacity and stiffness of the bearing. The parameters k_1 and H are important variables in the bearing design process, regarding the definition of stiffness and bearing load capacity.

Considering these results, one performed a case study in a grinding machine spindle, by modeling the shaft via finite

elements and the bearings with the present theory. Static and dynamic deflection maps are presented as a function of the bearing supply pressure, grinding force and depth of cut (maximum allowable deflection). These maps are useful tools in bearing design for defining the appropriated supply pressure and operational frequency range, given the values of grinding force and desired surface roughness (depth of cut).

It is important to emphasize that, these are numerical results whose model strongly depends on the simplifying hypotheses. The main limitation of this model lies on the hypotheses of fluid incompressibility and laminar flow regime. It is not certain, for instance, that the flow in the porous medium under a 2 or 3 *MPa* pressure supply condition still obeys such simplifying hypotheses. For this reason, experimental verification is mandatory. The first experimental studies are being carried out focusing on the identification of parameter k_1. This is important to check the values of k_1 adopted in the numerical simulations, and is the natural next step in model validation.

ACKNOWLEDGMENTS

The Brazilian research foundations FAPESP and CNPq are gratefully acknowledged for the support given to this project, as well as Prof. Carlos A. Fortulan for the advisory in ceramic material technology.

REFERENCES

Allaire, P.E., Parsell, J.A., Barret, L.E., 1981, "A Perturbation Method for the Dynamic Coefficients of Tilting-Pad Journal Bearings", Wear, Vol.72, pp.29-44.

Balestrero, L.A.P., 1997, "Uma avaliação de Mancais Aerostáticos para Máquinas Ferramentas: Estudo e Dimensionamento de Eixo Árvore", Universidade de São Paulo, Escola de Engenharia de São Carlos, Departamento de Engenharia Mecânica (D.Sc. thesis).

Cheng, K., Rowe, W. B., 1995, "A Selection Strategy for the Design of Externally Pressurized Journal Bearings", Tribology International, Vol.28, No.7, pp. 465-474.

Fortulan, C.A., 1997, "Influência dos Métodos de Injeção e de Prensagem Isostática no Desempenho das Cerâmicas Estruturais", Universidade de São Paulo, Escola de Engenharia de São Carlos, Departamento de Engenharia Mecânica (D.Sc. thesis).

Fourka, M., Bonis, M, 1997, "Comparison Between Externally Pressurized Gas Thrust Bearings with Different Orifice and Porous Feeding Systems", Wear, Vol.210, pp.311-317.

Hamrock, B.J., Schmid, S.R., Jacobson, B.O., 2004, "Fundamentals of Fluid Film Lubrication", McGraw-Hill Co., New York, 750p.

Kwan, Y.B.P., Corbett, J., 1998a, "A Simplified Method for the Correction of Velocity Slip and Inertia Effects in Porous Aerostatic Thrust Bearings", Tribology International, Vol.31, No.12, pp.779-786.

Kwan, Y.B.P., Corbett, J., 1998b, "Porous Aerostatic Bearings - An Updated review", Wear, Vol.222, pp.69-73.

Lo, C., Wang, C., Lee, Y., 2004, "Performance Analysis of High Speed Spindle Aerostatic Bearings", Tribology International, Vol.38, No.1, pp.5-14.

Majumdar, B.C., 1973, "Analysis of Externally Pressurized Gas Bearings with Journal Rotation", Wear, Vol.24, No.1, pp.15-22.

Majumdar, B.C., 1976, "Design of Externally Pressurized Gas-Lubricated Porous Journal Bearings", Tribology International, Vol.19, pp.71-74.

Majumdar, B.C., 1980, "Externally Pressurized Gas Bearings: A Review", Wear, Vol.62, pp.299-314.

Nelson, H.D., McVaugh, J.M., 1976, "The Dynamics of Rotor-Bearing Systems Using Finite Element", Trans. of ASME - J. Engineering for Industry, Vol.98, No.2, pp.593-600.

Nicoletti, R., Santos, I.F., 2005, "Frequency Response Analysis of an Actively Lubricated Rotor/Tilting-Pad Bearing System", Trans. of ASME - Journal of Engineering for Gas Turbine and Power, Vol.127, No.3, pp. 638-645.

Plante, J.S., Vogan, J., El-Aguizy, T., Slocum, A.H., 2005, "A Design Model for Circular Porous Air Bearings Using the 1D Generalized Flow Method", Precision Engineering, Vol.29, No.3, pp.336-346.

Powell, J.W., 1970, "Design of Aerostatic Bearings", The Machinery Publising Co., New York, 273p.

Roblee, J.W., Mote Jr., C.D., 1990, "Design of Externally Pressurized Gas Bearings for Stiffness and Damping", Tribology International, Vol.23, No.5, pp.333-345.

Sinhasan, R., Sharma, S.C., Jain, S.C., 1989, "Performance Characteristics of an Externally Pressurized Capillary-Compensated Flexible Journal Bearing", Tribology International, Vol.22, No.4, pp.282-293.

Sun, D.C., 1975, "Stability of Gas-Lubricated Externally Pressurized Porous Journal Bearings", Trans. of ASME - J. of Lubrication Technology, Vol.97, pp. 494-505.

Yoshimoto, S., Kohno, K, 2001, "Static and Dynamic Characteristics of Aerostatic Circular Porous Thrust Bearings", Trans. of ASME - J. of Tribology, Vol.123, No.3, pp.501-507.

Zhou, L., Syoji, K., Kuriyagawa, T., 1992, "Ceramic Mirror Grinding: Using Extremely Fine Grit Diamond Wheel", Proc. of 7th. Annual Meeting of The American Society for Precision Engineering, Grenelefe, USA, pp.79-82.

RESPONSIBILITY NOTICE

The authors are the only responsible for the printed material included in this paper.